Aksaker *et al.*
Progress in Earth and Planetary Science (2026) 13:2
https://doi.org/10.1186/s40645-025-00739-x

Progress in Earth and Planetary Science

RESEARCH ARTICLE Open Access

Light pollution trends for International Dark Sky Places using VIIRS nighttime light composite data

Nazım Aksaker[1,2*], Murat Bayazıt[3], Zühal Kurt[2], Sinan Kaan Yerli[4] and Mehmet Akif Erdoğan[5]

Abstract International Dark-Sky Places (IDSPs) is a global project led by the International Dark-Sky Association (IDA) to protect dark-sky areas for astronomical observation and astro-tourism. Currently, there are 216 IDSPs in the world. This study analyses light pollution trends in International Dark-Sky Places (IDSPs) using VIIRS night light composite data. IDSPs are mostly located near urbanised areas in Europe and away from urbanisation in North America. Dark and large areas away from urbanisation in South America, Africa, Central Asia and Australia offer great potential. Linear regression analysis shows that in 94% out of 216 places there is no change in artificial light at nigh (ALAN). There is a decrease in the level of artificial light in 3% and an increase in the level of artificial light in 3%. Unlike the linear regression analysis, Mann–Kendall and Sen slope analyses revealed significant statistical changes at the 105 sites (78 increasing and 27 decreasing). Machine learning models including decision tree regression (DTR), random forest regression (RFR) and gradient boosting regression (GBR) provided good predictive accuracy ($R^2 > 0.6$). Seasonal patterns were assessed using the Lomb–Scargle periodogram, but detected periodicities were considered false positives. These results emphasise the need for strategic planning to reduce light pollution in IDSPs, especially in underused areas.

Keywords International Dark Sky Places, Light pollution, Machine learning, Statistical models, Mann–Kendall test, Lomb–Scargle periodogram

*Correspondence:
Nazım Aksaker
naksaker@cu.edu.tr
[1] Adana Organised Industrial Zones Vocational School of Technical Science, Çukurova University, 01410 Adana, Türkiye
[2] Space Science and Solar Energy Research and Application Center (UZAYMER), Çukurova University, 01330 Adana, Türkiye
[3] Republic of Türkiye Ministry of Foreign Affairs, Dr. Sadık Ahmet Street. No:8 Balgat, 06520 Ankara, Türkiye
[4] Department of Physics, Orta Doğu Teknik Üniversitesi, 06800 Ankara, Türkiye
[5] Faculty of Architecture, Landscape Architecture Department, Hatay Mustafa Kemal University, 03160 Hatay, Türkiye

© The Author(s) 2026, modified publication 2026. **Open Access** This article is licensed under a Creative Commons Attribution 4.0 International License, which permits use, sharing, adaptation, distribution and reproduction in any medium or format, as long as you give appropriate credit to the original author(s) and the source, provide a link to the Creative Commons licence, and indicate if changes were made. The images or other third party material in this article are included in the article's Creative Commons licence, unless indicated otherwise in a credit line to the material. If material is not included in the article's Creative Commons licence and your intended use is not permitted by statutory regulation or exceeds the permitted use, you will need to obtain permission directly from the copyright holder. To view a copy of this licence, visit http://creativecommons.org/licenses/by/4.0/.

1 Introduction

Light pollution is defined as the disturbance of the natural illumination that exists at night by anthropogenic light sources (Falchi et al. 2016). This negative effect is known as artificial light at night and is abbreviated as ALAN (Green et al. 2022).

During the past decade, the global average increase in light pollution has been 2 per cent per year in both the illuminated area and total luminance. This rate is approximately twice the rate of growth of the world population (Kyba et al. 2017). Several factors contribute to the accelerated growth of light pollution, including population growth, economic growth, income growth, gross domestic product and migration (Henderson et al. 2012; Yerli et al. 2021; Phan 2023).

The phenomenon of light pollution has been identified as having a multitude of adverse effects on living organisms. Several studies have identified some adverse effects of light pollution on humans, animals and plants (Longcore and Rich 2004; Cao et al. 2023; Sun et al. 2024). ALAN affects the feeding, mating, migration, communication, competition and hunting habits of animals, including insects, birds, reptiles, amphibians and even fish Grubisic et al. (2018); Owens et al. (2020). Light pollution can also disrupt the natural cycles of plants, affecting when they sprout, bloom, enter dormancy and lose their leaves. This can lead to changes in how communities of plants and animals interact with each other, which can disrupt the ecosystem Singhal et al. (2019).

There are many different ways that light pollution can affect people Paksarian et al. (2020); Argys et al. (2021). Humans are able to synchronise their own biological clock with the Earth's cycle of day and night Gaston and Sánchez de Miguel (2022). Disruptions to this process can lead to an increase in the number of people suffering from diseases like vision loss, metabolic disorders, diabetes, obesity, coronary heart disease, tumours and even cancer, depending on their melatonin levels Fonken et al. (2013); Zubidat and Haim (2017); Grubisic et al. (2019)

In the field of astronomy, it is well known that light pollution negatively affects the quality of observation results Rodrigo-Comino et al. (2023). The visibility of stars is significantly affected by light pollution, with the number of observed sources decreasing logarithmically with increasing levels of pollution (Cinzano et al. 2000; Falchi et al. 2016).

Light pollution is distributed differently across continents, with levels often being related to urbanisation and economic development Falchi et al. (2019). Currently, 80% of the Earth's population is exposed to light pollution, and one-third of the population today cannot observe the Milky Way Galaxy with the naked eye (Falchi et al. 2016).

To avoid the negative effects of light pollution in the future, it is crucial to move away from areas with high pollution potential to more natural areas and to utilise resources efficiently.

A multitude of techniques have been used so far to quantify light pollution. These can be broadly classified into two categories: those conducted in the air and those conducted on the ground. Ground-based techniques encompass digital cameras (Barentine et al. 2020), light measuring devices (Hänel et al. 2018), the TESS-W instrument (Zamorano et al. 2019) and SQM instruments (Falchi et al. 2016). Among these, the SQM instrument is the most prevalent. Its accessibility and cost-effectiveness have contributed to its popularity. This technique is frequently used in the "dark sky park certification" process (Barentine 2016; Lima et al. 2016; Papalambrou and Doulos 2019; Marr 2024). Although it is a highly useful technique in small areas, it becomes less effective as the areas become larger (Mander et al. 2023). Examples of space-borne measurement techniques include satellites (Kyba et al. 2014; Barentine et al. 2021) and space photographs taken by astronauts from the ISS (Schirmer et al. 2019). Satellite measurements provide the most systematic data, facilitating measurements over large areas and enabling time series analyses (Zhao et al. 2019).

The International Dark Sky Association (IDA) was established in 1988 by professional astronomer David Crawford and amateur astronomer Tim Hunter to protect dark skies. There is a process carried out by IDA in line with certain criteria for the identification of dark sky areas. Currently, there are over 160000 square kilometres of protected land and night skies in 22 countries on six continents, with the number of certified locations (named "International Dark Sky Places", IDSPs) increasing annually. The 216 certified IDSPs are plotted in Fig. 1, and their properties (longitude, latitude, area, country, date and category) are given as a supplement collected from the IDA website (`darksky.org`); 10 of them are tabulated in Table 1. This table is ordered from largest to smallest by area.

These areas are important for tourism and have a mission to protect dark skies and economic returns (Mitchell and Gallaway 2019; Escario-Sierra et al. 2022; Iwanicki 2022). The interest in IDSPs is growing day by day. This is a very promising process for astro-tourism and astronomy.

Based on ground measurements, it is known that these areas have at least the status of "dark skies". With urban sprawl reaching rural areas and population growth (Mu et al. 2021; Xiang and Tan 2017; Amaral et al. 2006), it is important to know how many of these important places are exposed to ALAN. Light pollution is a complex topic influenced by various factors, including urban lighting,

light sources such as ski resorts and factories, the dispersion of aerosols, clouds, snow and moonlight Wallner and Kocifaj (2023); Liu et al. (2020); Kyba et al. (2011). Therefore, as urban centres grow, the areas that need to be protected from light pollution also increase.

For IDSPs, measurements taken before obtaining park status are usually *in situ* measurements, such as SQM measurements and all-sky imagery. Kyba and Coesfeld (2021) used satellite data for 98 parks, emphasising the temporal variation of changes in light emission and shifting the focus to satellite data. In contrast to the classical area analysis method with SQM, this study used satellite imagery covering a larger area and obtained the most up-to-date temporal statistics for 216 places.

The main objective of this study is to show the increasing or decreasing trends of artificial light levels in certified dark sky areas over the last decade. This will be achieved by using satellite-based remote sensing data and statistical methods to identify and quantify temporal changes in light pollution. This study highlights the light pollution of IDSPs around the world over the last decade and, for the first time, provides temporal variations in light pollution of certified international IDSPs. In addition, different regression models were used: the Mann–Kendall test statistic and Sen's slope coefficient were used to calculate whether the changes were significant, and the LS method was used to examine whether there is a periodic change. This is the first study to examine the darkness trends in certified international IDSPs using satellite data worldwide.

2 Methods and data reduction

The investigation of light pollution in IDSPs involves several key steps: creating a database, correcting and transforming the data, and performing statistical analyses and interpretations. The flow chart of this study is illustrated in Fig. 2.

2.1 The acquired data

The data utilised in this study are day–night band (DNB) detected data from the Visible Infrared Imaging Radiometer Suite (VIIRS) instrument on the Suomi National Polar-Orbiting Partnership (Suomi NPP) satellite, which is in the sun-synchronous polar orbit with the Sun at an altitude of 833 km above Earth Liao et al. (2013). The DNB provides visible and near-infrared spectral images of the Earth, which are panchromatic, and it has a wavelength coverage of 0.5—0.9 μm. Due to its superior signal-to-noise ratio at low brightness levels and nearly constant footprint over the entire field, DNB data are uniquely suited for studying city lights Cao and Bai (2014a).

DNB values are in units of W cm^{-2} sr^{-1}. The instrument is capable of recording data with a radiometric resolution of 12 bits and a local resolution of 750 ms, with two passes per day from the same location, both day and night Hillger et al. (2013). The spatial resolution of the geographical information system (GIS) dataset produced daily is 742 m per pixel, with a total area of 3060 km shown in a single frame Elvidge et al. (2013).

Data for this study were acquired from the relevant Earth Observation Group (EOG) website. The data cover the period from 2012 to 2022, with approximately 3930 nights. During this period, 129 GeoTIFF images (129×11 GB $\cong$ 1.5 TB) were acquired.

2.2 Data preprocessing

Artificial light data from the day–night band (DNB) of the Visible and Infrared Imaging Suite (VIIRS) instrument on the Defence Meteorological Satellite Program (DMSP) satellites are available in different versions (monthly, yearly, tiled, non-tiled, etc.). The VIIRS Nighttime Lights (VNL) used in this study provide Version 1 (V1) composite, monthly data with stray light corrections by Elvidge et al. (2021). It should be noted, however, that airglow corrections are not included. For the dataset with a GeoTIFF extension, Coesfeld et al. (2020)'s correction files with CSV extensions were used. The correction files applied for artificial light in this study were obtained from *lightpollutionmap.info*, an online platform operated and continuously updated by Jurij Stare. This dataset continues to be produced on an ongoing basis. The files obtained from this source were converted to raster files with the `ASC` extension and geo-located by adding the WGS84 coordinate system using ArcGIS Pro 3.4.

As given in the second step in the flow chart in Fig. 2, airglow raster data were then subtracted from VNL/V1 data for each month and each year to obtain corrected data. In addition to these processes, it should be noted that there were negative values in the final version of the data, which cannot be accepted as brightness. Consequently, these pixels were not considered and assigned a value of "NO DATA". Subsequently, given the presence of a northern light effect in the regions near the North Pole, which yielded statistically insignificant results to global light pollution, a mask dataset for the northern lights was employed, the corresponding locations being changed to "NO DATA": third stage in Fig. 2 (Elvidge et al. 2020). This masking process is for visual purposes and was not incorporated into the data processing.

The night sky brightness values measured by SQMs are represented by mag arcsec^{-2} unit (Cao and Bai 2014b). However, since no filter is assigned to SQM measurements, they are denoted by mag_{SQM} arcsec^{-2} (Puschnig et al. 2014).

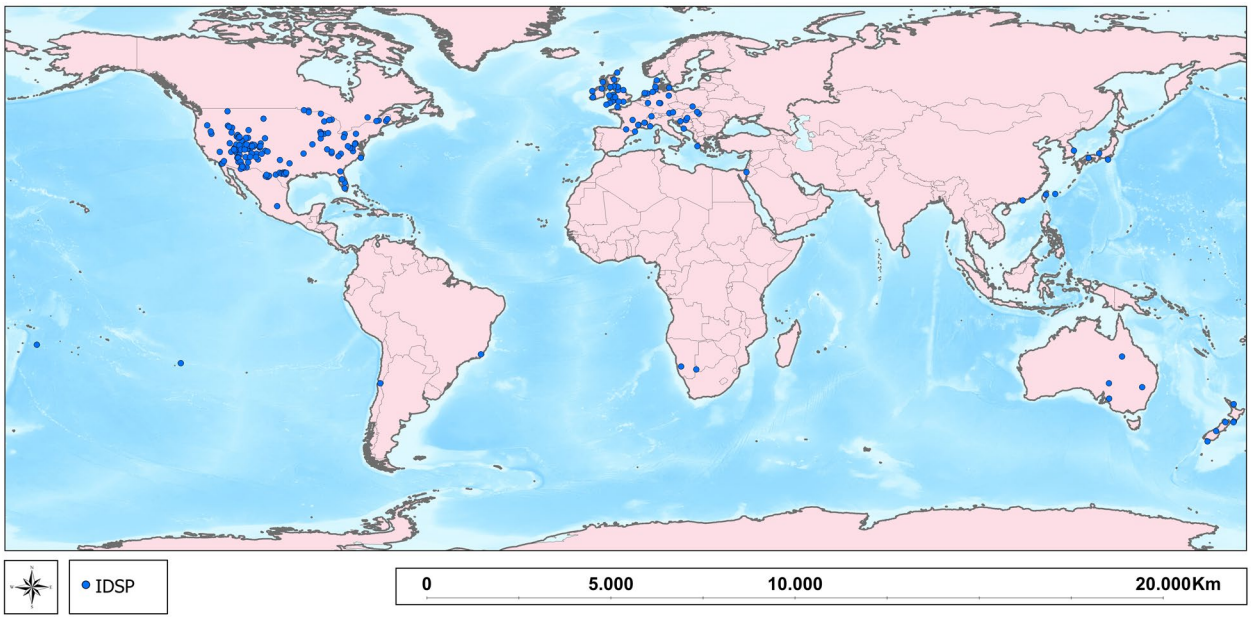


Fig. 1 Distribution of IDSPs. They are marked with blue dots

The map in Fig. 3 shows the ALAN, where the radiation unit is nW cm^{-2} sr^{-1}. To visualise the astronomical quality of the geographical area under study, we have expressed the area in terms of SQM magnitude (mag $arcsec^{-2}$) expressed in units of nW cm^{-2} sr^{-1} for use in Figs. 3 and 6. These figures were converted to SQM units of mag_{SQM} $arcsec^{-2}$ using the following equation (Aksaker et al. 2020; Sanchez de Miguel et al. 2020): $SQM = 20.0 - 1.9 \times \log(AL)$. Figure 3 presents an image of the world captured by the VIIRS/DNB instrument in 2022, overlaid with a map of the IDSPs approved by the IDA. In the figure, the categorically white to black colour gradient represents a contrast of high brightness to low brightness and category ranges determined according to a study of Martínez-Ledesma et al. (2019).

2.3 Mapping the ALAN

In the mapping process, the "Layout View" screen in ArcGIS Pro 3.4 was used. At this stage, each data frame was placed in an orderly manner and different maps were positioned side by side or below each other on a single page. In order to increase the readability and visual integrity of the map, basic cartographic elements such as a north arrow, scale bar, legend and title were added to each map. Legends are customised to clearly identify the classes and symbols shown, and scale bars are set in metric units in accordance with the level of detail of the map. Text boxes ("text") and annotations ("annotation") have been used to make the maps more comprehensible, and icon sizes and fonts have been arranged with visual balance in mind. By reviewing the background colour, frame

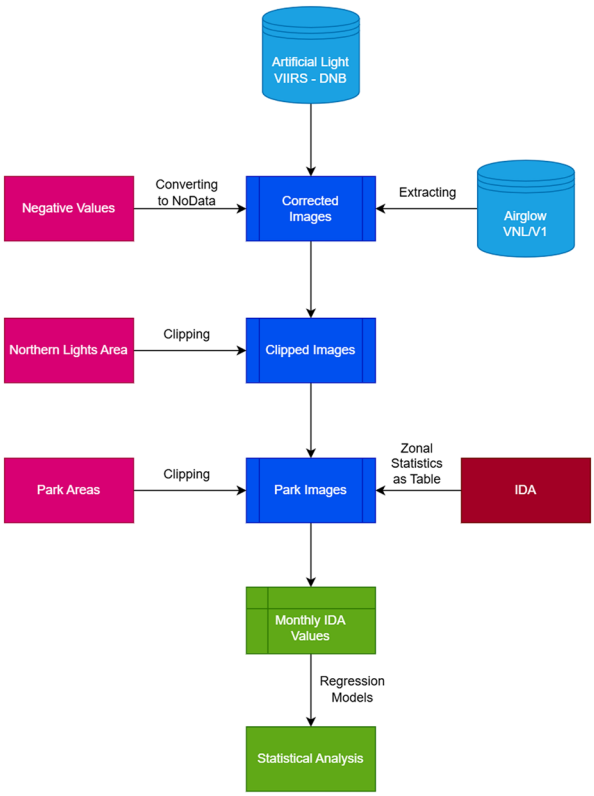


Fig. 2 Flow chart of data analysis carried out in this study

lines and spacing settings, all sub-maps were aligned as a single whole and a visually harmonious presentation was created within this integrity. Finally, the output was exported in high-resolution PDF format with the "Export Map" tool.

2.4 Analysis

The temporal statistics of the IDSPs certified by IDA were extracted using ArcGIS Pro 3.4 GIS software, using monthly images obtained from satellite imagery that span from 2012 to 2022 (the fifth stage in Fig. 2). A total of 129 monthly light pollution images in GeoTIFF format were analysed, with the ALAN values of the sites obtained through the use of a vector format dataset containing the latitude and longitude values of the IDSPs. The vector dataset containing the boundaries of IDSPs was obtained from Spinner et al. (2024). The process involved the utilisation of the "Zonal Statistics as Table" tool, which reads the spatial values of a feature in a relevant location in the raster image, plus using batching methods to facilitate automation of spatial analysis and data management procedures for all data. The outcome of this process was the acquisition of all spatial monthly ALAN values of IDSPs between the years 2012 and 2022. Outlier values caused by either missing satellite coverage on IDSP locations or abrupt temporal variations have been cleared out from all frames in all datasets.

2.5 Statistical analysis

At this stage, the last one in Fig. 2, the annual average light pollution values of IDSPs were obtained, and statistical inferences were made for this time series covering the period 2012–2022. To begin with descriptive statistics such as standard deviation, maximum, minimum and mean were obtained for this dataset (Table 2). In the next steps, missing values in the time series are linearly interpolated to ensure completeness. The time index was the independent variable. Data values are the dependent variable here. This approach made it possible to determine the regression coefficients, which were then used to construct the regression equation.

Different statistical methods were used using annual average data to determine changes in light pollution at 216 sites where IDSPs are located. The first is the commonly used linear regression (Aksaker et al. 2020; Yerli et al. 2021). Table 2 presents the linear regression equation and R^2 value obtained for IDSPs. The R^2 value is between 0 and 1 and the higher the value, the stronger the relationship (Rees and Rees 1989). Linear regression is based on the assumption that the dataset is normally distributed (Poole and O'Farrell 1971). Independent of this assumption, the Mann–Kendall test statistic was also calculated in this study (Mann 1945; Kendall 1975). Although the Mann–Kendall test statistic is used primarily for changes in atmospheric parameters, it has also been used to determine whether the change in ALAN over time is significant (He et al. 2013; LaRoe et al. 2022). The Mann–Kendall test statistic p is nonparametric and is based on the assumption that the data are non-normally distributed (Conover 1999). If the p-value obtained is greater than 0.05, it is said that there is a significant change in the time series. In addition to the Mann–Kendall test statistic, the Sen slope coefficient Q indicates the amount of slope in a nonparametric time series by Sen (1968). If this number is negative, it means that the time series is changing in a negative direction, and if it is positive, it means that the time series is changing in a positive direction (Pohlert 2016). The coefficient values a, b and R^2 were obtained from linear regression, Mann–Kendall test statistic (MK) and Sen's slope coefficient (Q) and are given in Table 2. MK and Q values were calculated using the software `RStudio`. The obtained MK and Q values are also visualised in Fig. 4 by using the locations of the sites on the world map. In this way, the areas of change can be seen more clearly.

According to the coefficient obtained from the linear regression equation, the two places with the highest positive and negative change were selected and graphed. These graphs are presented in Fig. 5. Linear regression plots for all IDSPs are given in appendix. In addition to these statistics, averaged annual development (AAD) and averaged pixel value (AVP) over 10 years of statistics based on Wallner et al. (2023) were also calculated and added to Table 2. We also plotted the SQM comparison values for three IDSPs with the changes between 2012 and 2022 (Fig. 6).

2.6 Regressions with machine learning

In this study, a series of regression models are implemented and evaluated to predict time series data from radiance in IDSPs. The dataset containing the dates and corresponding radiance values is preprocessed and divided into training, validation and test sets. Specifically, every 10 rows are allocated to the test set, while the remaining rows are used for training and validation. The training data were further divided into training and validation subsets using an 80–20 ratio. Several machine learning regression techniques from the `scikit-learn` Python library are employed to predict radiance values based on the monthly dataset. These include linear regression, which serves as a baseline by assuming a linear relationship between features and the target variable; Ridge regression, an extension of linear regression that incorporates regularisation of L2 to penalise large coefficients and mitigate multicollinearity (Sysoev and Burdakov 2019); and Lasso regression, which uses regularisation of L1 for feature selection by driving some coefficients to zero. ElasticNet

combines regularisations (L1 and L2) to balance the advantages of Lasso and Ridge regressions (Gana 2022). Support vector regression (SVR) is utilised to capture complex relationships by finding the optimal hyperplane that fits the data within a specified margin of tolerance (Basak et al. 2007). Furthermore, random forest regression, an ensemble learning method, aggregates predictions from multiple decision trees to reduce overfitting and improve robustness (Altman and Krzywinski 2017), and gradient boosting regression, which builds models sequentially and corrects errors of its predecessors through gradient descent optimisation, is also applied (Natekin and Knoll 2013).

Each model is trained in the training set and tuned using the validation set to optimise hyperparameters and prevent overfitting. The models are subsequently evaluated on the test set using performance metrics, with a primary focus on the R-squared (R^2) score, which measures the proportion of variance in the dependent variable explained by the model. Performance metrics for each regression model, including R^2 scores, are documented and summarised in Table 3, providing a comparative analysis of their predictive performance. Among the tested 12 models, DTR, RFR and GBR models showed substantially higher R^2 scores (Fig. 7). We also plot DTR, RFR and GBR for Groveland/USA in Fig. 8.

2.7 Lomb–scargle periodogram

The Lomb–Scargle (LS) method was used to search for periodicity in IDSP monthly ALAN values. The LS periodogram is a method that is often used to resolve problems in time series analysis in astronomy (Lomb 1976; Scargle 1982). The raw values of the IDSPs are read to represent different geographical locations. Missing values in the time series were interpolated using linear methods to ensure data continuity. To detect periodic signals, the LS periodogram was applied to the radiance time series data with these settings. The frequency corresponding to the maximum power was identified as the dominant frequency, and the period was calculated as the reciprocal of this frequency (Schwarzenberg-Czerny 1998). The statistical significance of the detected periodicity was assessed by computing the false alarm probability (FAP) (Baluev 2008). The results are given in Fig. 9, and the tabular results include the period, FAP and maximum power given in Table 4.

3 Results and discussion

3.1 General situation

The global locations of IDSPs are presented in Fig. 1. These 216 locations, which are the subject of this study, are given on the global map with blue dots. Existing dark-sky sites seem to be closer to the light areas clustered in North America and European countries. There are no IDSPs in mostly dark deserts or mountains. This may be due to transport and human access. However, IDSPs located in easily accessible places are affected by the ALAN around them over time. 61% of these locations are located in the USA. The largest area of these sites is the Greater Big Band International Dark Sky Reserve in the USA covering 54336.57 km^2. These sites include 119 parks, 44 communities, 25 reserves, 19 sanctuaries and nine urban night sky sites. In 2021, there were 34 areas certified, the most compared to any other year, followed by 26 areas in 2019. The 10 parks listed in Table 1 are ordered from largest to smallest area. The 2022 VIIRS image is given in Fig. 3. As can be seen in the legend of the map, the image consists of 8 categories. As expected, regions with higher urbanisation and human footprints such as India, China, the USA and Europe exhibit more ALAN. There are four different classes defined by the IDA. These are Settlement Area, Reserve Area, International Dark Sky Park and Conservation Area (Kurt et al. 2024). According to these classes, Dark Sky Parks are located between 21.2–21.5 mag_{SQM} $arcsec^{-2}$. Values with magnitudes in this range are spread over an area of 90%. These areas are South America, Africa, Central Asia, Australia and the oceans. Similarly to Figs. 1, 4 shows that existing IDSPs are primarily located near brightly lit regions in North America and European countries. Notably, there is no Dark Sky.

3.2 Linear regression and statistics

All descriptive statistics and Mann–Kendall and Sen slope statistics are given in Table 2. The place with the highest value among all IDSPs is Parc du Mont-Bellevue in Canada with 57.94 nW $cm^{-2}sr^{-1}$. Out of 216 sites, the Medicine Rocks State Park, in the USA, has the lowest value (~0.0). The site with the lowest AAD is the Greater Big Bend International Dark Sky Reserve (−606.37). The highest APV value is Stacy Park with a value of 23.69 nW cm^{-2} sr^{-1}. The lowest value for this statistic is Medicine Rocks State Park with a value of −0.14 nW cm^{-2} sr^{-1}. The highest average value is at Stacy Park with 26.02 nW cm^{-2} sr^{-1} and the lowest is at Chiricahua National Monument with ~0.0 nW cm^{-2} sr^{-1}. The location with the highest value in R^2 obtained from the linear regression equation calculated assuming that the sample is normally distributed (see Sect. 2.5) is Groveland, USA (0.68). However, of 216 locations, only Groveland obtained an R^2 value above 0.5. The nonparametric Mann–Kendall and Sen's slope statistics, calculated under the assumption that the dataset has a non-normal distribution (see Sect. 2.5), indicate whether the changes in these positions are statistically significant and, if so, in what direction. Of these 105 locations, 78 showed an upward trend, while 27 showed a downward trend. This means that

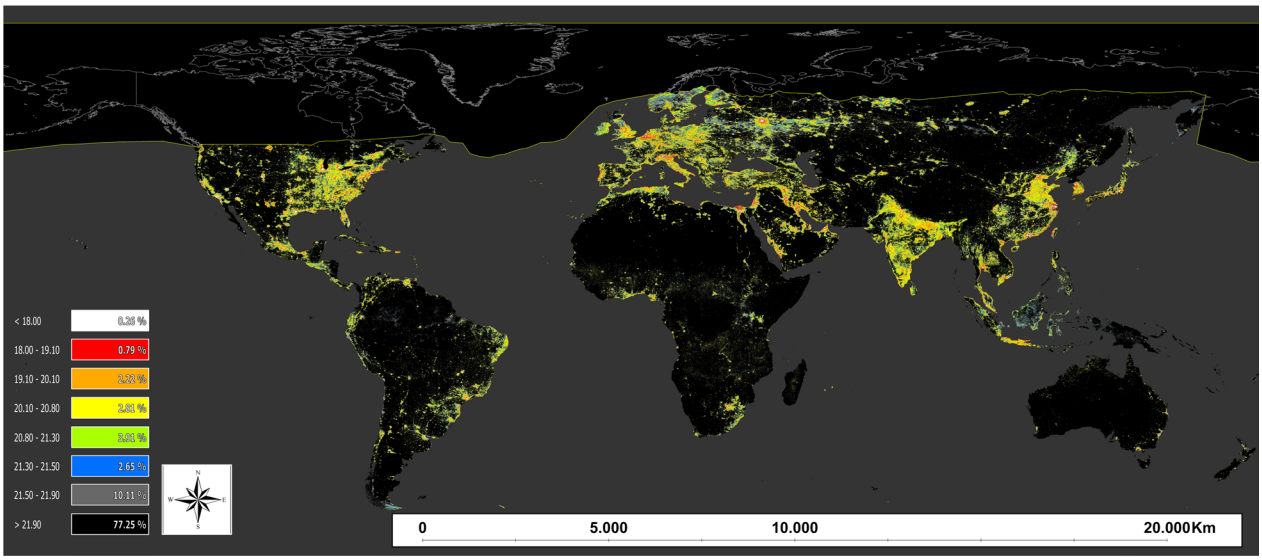


Fig. 3 The image shows SQM values all over the world in 2022. Lower values mean bright areas and higher values mean dark areas. Legend is provided to show different categories of data. White areas are highest light polluted areas and black areas are the least. Every category coverage percentage is given in the related colour bar. To avoid noise in the Northern Pole, a Northern Light boundary was applied for masking (yellow boundary)

light pollution has increased in 78 IDSPs and decreased in 27 IDSPs. These results are indicated by arrows in the last column of Table 2 and are also shown on the map in Fig. 4. Sites with increasing or decreasing light pollution do not show a specific geographical pattern. Although it is difficult to conclude the less widespread IDSPs in Brazil, Africa and Australia, the data clearly show that most IDSPs in Europe are trending upwards. In the studies by Aksaker et al. (2020), Yerli et al. (2021) and Wallner et al. (2023) localised increases are analysed in detail together with their causes and demographic correlates such as population density and gross domestic product

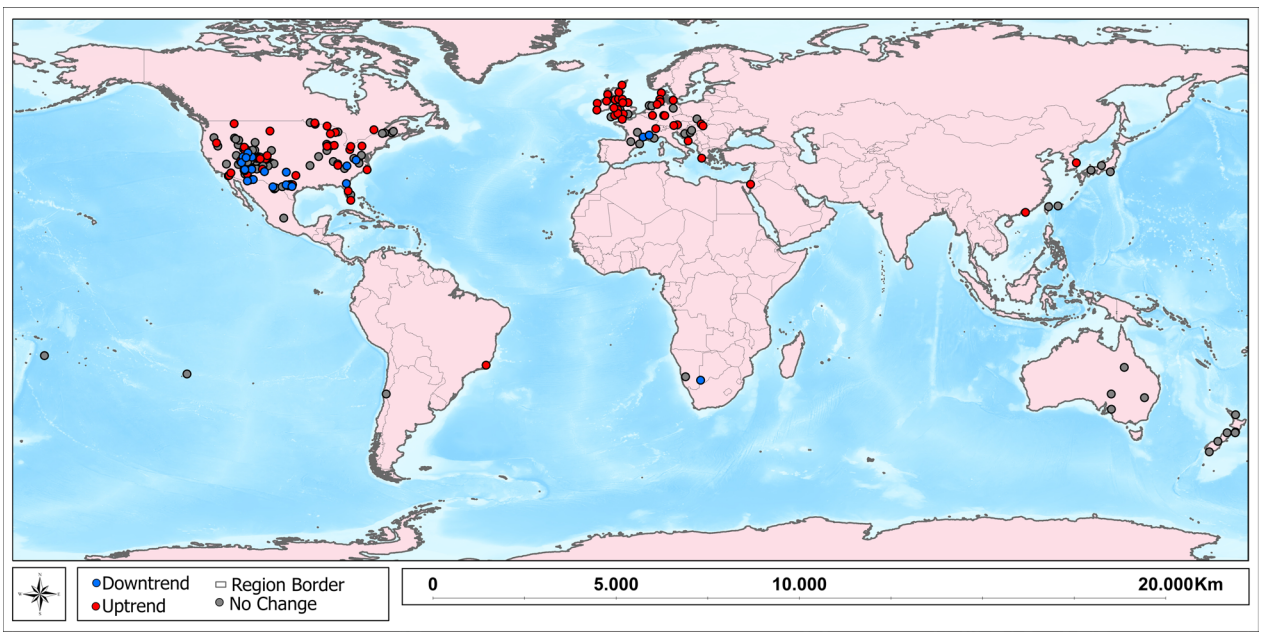


Fig. 4 Mann–Kendall statistics calculations over the world map. Pink areas show world political boundaries and for statistically meaningful results; grey points show no change; blue points show a downtrend; and red points show an uptrend

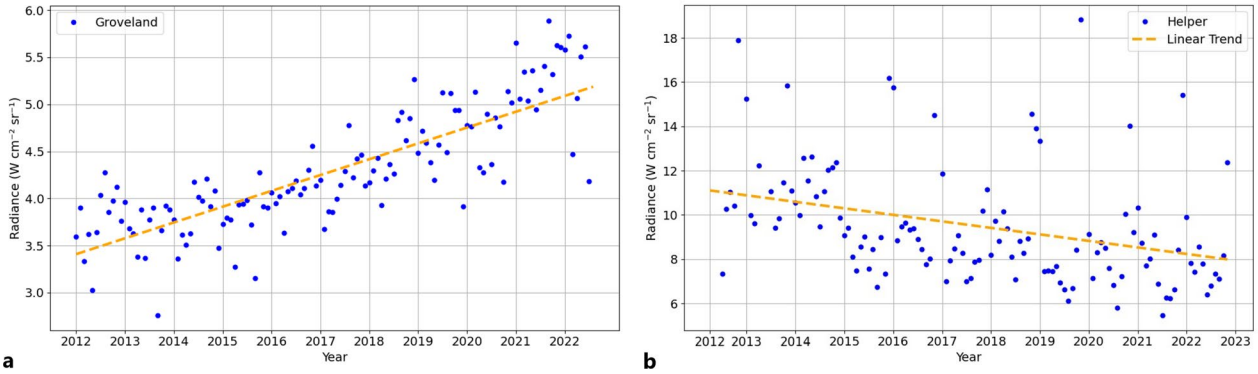


Fig. 5 Slope values of the places, which are two of the places that show the most variability with the linear regression method calculated over the point-based pixel value (**a**, **b**). Blue lines represent data values, and orange dashed lines represent linear regression trend lines. The full list of linear regressions for all IDSPs can be found in Appendix

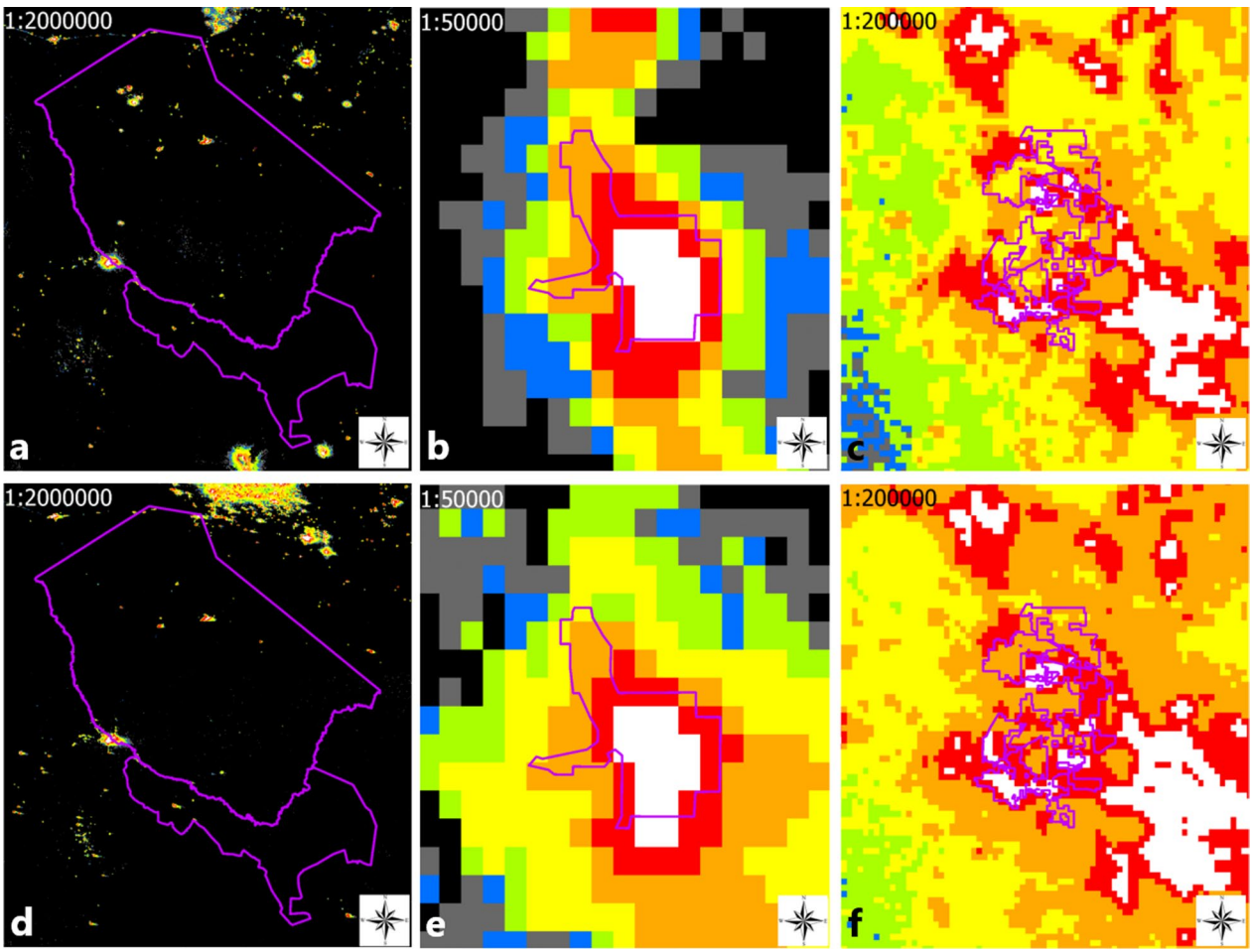


Fig. 6 The plots compare SQM values for places with the changes between 2012 (**a**–**c**) and 2022 (**d**–**f**). At the left is "Greater Big Bend International Dark Sky Reserve", the largest place (**a**, **d**). In the middle is Helper, which experienced a negative change (**b**, **e**) and at the right is Groveland showing a positive change (**c**, **f**). The colour bar below categorises SQM values from black (darkest) to white (brightest). The colour index is the same as Fig. 4

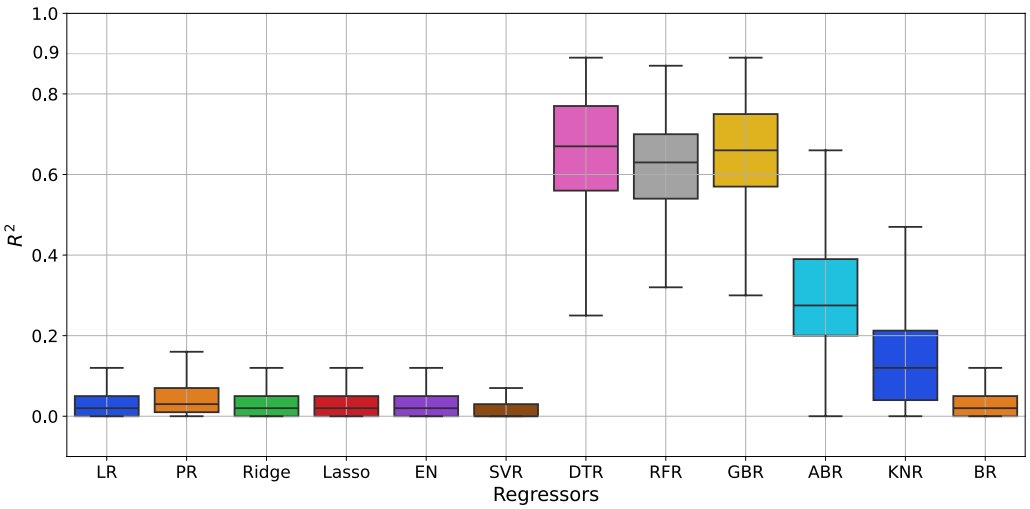


Fig. 7 Boxplot comparing R^2 scores across regression models. Box colours represent models, with the middle line showing the mean of R^2 score IDSP values. Error bars indicate the standard deviation of the R^2 score for IDSP

are mentioned. These studies show that the population density and development levels of countries are directly proportional to ALAN. This indicates that these areas are becoming increasingly unsuitable for astronomical observations. In contrast, the USA, which has the largest number of IDSPs, shows predominantly no trend, with some sites showing an upward trend. Linear regression and the Mann–Kendall test are inherently subject to certain limitations and assumptions in the calculation of the fit. Therefore, 12 different regression models for the time series in this study were calculated (Table 3). A total of 12 different regression models, including linear regression, were applied to this time series, and three regression methods gave high R^2 values. These are decision tree regression (DTR), random forest regression (RFR) and gradient boosting regression (GBR). All three models are based on decision trees, all are supervised learning techniques, and all three can model nonlinear relationships. As a result, they make better sense of complex data structures. It should be noted that all three regression methods are nonparametric. Figure 8 shows how all these regression methods perform in terms of the R^2 score. These techniques have previously been used for the variation and prediction of ALAN (Sainger et al. 2020; Zou et al. 2023; Zheng et al. 2023). In this study, these three techniques are recommended because they give better results than the others.

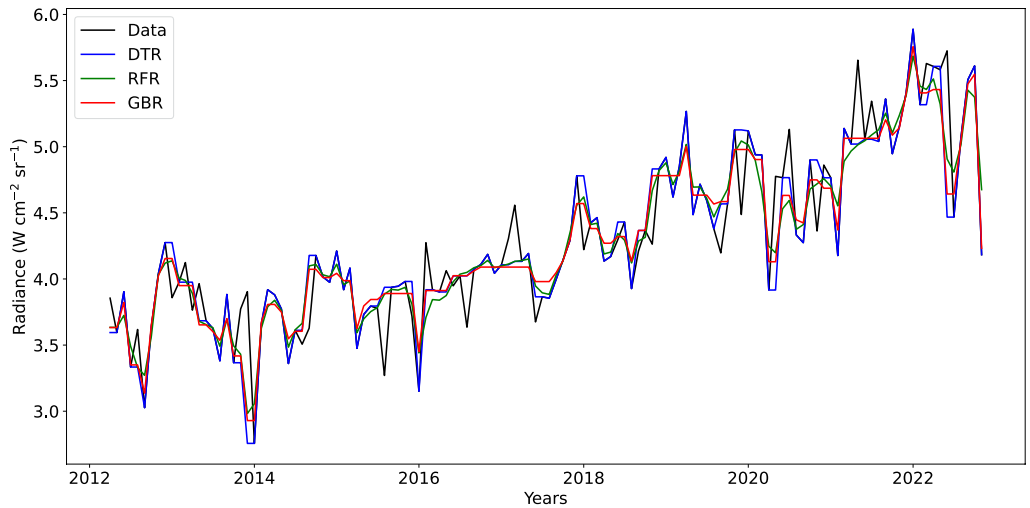


Fig. 8 The light trend for Groveland was plotted using regression algorithms, including DTR, RFR and GBR

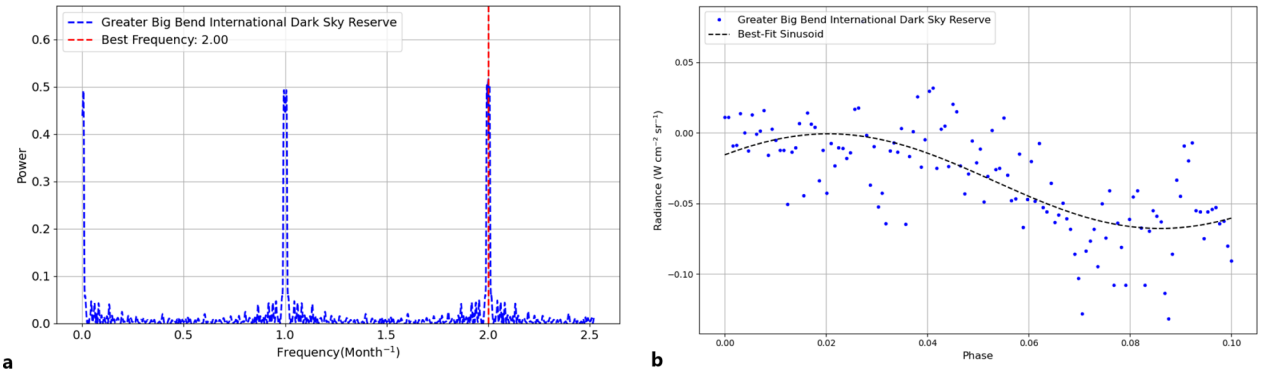


Fig. 9 Lomb–Scargle power and folded plot of Greater Big Bend International Dark Sky Reserve place **a** The blue lines represent Lomb–Scargle periodogram curves. The red line indicates this method's most probable peak and corresponding frequency value. **b** The blue dots represent the radiance values, while the black dashed line shows the best-fit sinusoid curve for these points

Table 1 Fundamental properties of selected IDSPs

Site	Longitude	Latitude	Area (km^2)	Country	Date
Greater Big Bend International Dark Sky Reserve	− 103.62	29.84	54336.57	USA, Mexico	2022
Death Valley National Park	− 117.13	− 117.13	21325.15	USA	2013
Oregon Outback (Lake County, Phase One)	− 120.00	− 120.00	18604.95	USA	2024
Kerry	− 9.72	− 9.72	12745.40	Ireland	2014
Quetico Provincial Park	− 91.50	− 91.50	10713.63	Canada	2021
Mont-Mégantic	− 71.25	−7 1.25	10712.05	Canada	2007
Boundary Waters Canoe Area Wilderness	− 91.39	− 91.39	9935.51	USA	2020
Aoraki Mackenzie	170.33	170.33	9226.37	New Zealand	2012
Grand Canyon National Park	− 112.68	− 112.68	7486.94	USA	2016
Cévennes National Park Buffer Zone	3.72	3.72	7313.75	France	2018

The latitude and longitude are in degrees, the area is in km^2, and the date is the year of designation of the place. The list is sorted from largest to smallest by area

3.3 Temporal variations

Figure 5 shows the annual temporal variation of the two sites with the highest linear regression slopes for the two sites, Groveland and Helper. The Groveland (left panel) showed an increasing trend, while Helper (right panel) showed a decreasing trend. The areas shown in purple represent the IDA areas. Figure 6 compares the SQM values between 2012 and 2022 for the three sites. The top panel shows satellite images of ALAN in 2012 and the bottom panel in 2022. "Greater Big Bend International Dark Sky Reserve" (Fig. 6a, d) remains the largest site. "Helper" (Fig. 6b, e) shows a negative change with increasing brightness (a: −0.02). "Groveland" (Fig. 6c and f) shows a positive change with a slight improvement in darkness (a:0.01). To determine whether the peaks in ALAN increases are significant or recurring due to seasonal effects, the best frequency values for all sites were determined using the LS periodogram. In the case of "Greater Big Bend International Dark Sky Reserve", most of the increases were periodic, with notable peaks at frequencies corresponding to 0, 1 and 2 months. These peaks are more prominent and significant than others (Fig. 9). The power values obtained from the LS periodograms are presented in Table 4 for the 10 IDSPs, together with the corresponding false alarm probability (FAP) values indicating the accuracy of the detected peaks. Although periodic patterns were detected in the analysis, these were considered false positives as the values were consistent with the monthly sampling interval. The analysis of IDSPs has provided important information on the relationship between urbanisation, light pollution and the effectiveness of IDSPs in protecting dark skies. The proximity of many IDSPs to bright urban areas, especially in North America and Europe, has a dual effect: it increases accessibility but also compromises the quality of observations due to high levels of AL. This trend is evident in the comparison of values and the spatial distribution of IDSP sites by urbanised areas. We also note that large, remote areas without public access, such as deserts, are generally not suitable for the IDSP programme. Although these areas may align with the criteria for the

Table 2 Statistics of the dataset for the selected IDSPs

Places	Min.	Ave.	Max.	σ	2012	2022	APV	AAD	a	b	R^2	MK	Q	
Greater Big Bend International Dark Sky Reserve	−0.13	−0.03	0.08	0.04	0.00	−0.06	0.00	−606.37	0.00	0.01	0.44	0	−6.00E−04	↓
Death Valley National Park	−0.08	0.02	0.25	0.05	0.01	0.02	0.00	34.23	0.00	0.02	0.00	0.66	0.00E+00	–
Oregon Outback (Lake County, Phase One)	−0.15	0.03	0.40	0.09	−0.01	0.01	0.01	−32.14	0.00	−0.01	0.06	0.03	2.00E−04	↑
Kerry	−0.13	0.45	1.42	0.27	0.27	0.49	0.24	8.04	0.00	0.36	0.03	0	1.00E−03	↑
Quetico Provincial Park	−0.12	0.10	0.67	0.17	−0.01	0.13	−0.01	−120.23	0.00	0.04	0.04	0	6.00E−04	↑
Mont-Mégantic	0.54	1.22	2.55	0.57	0.83	1.31	1.05	5.90	0.00	1.22	0.00	0.1	2.00E−03	–
Boundary Waters Canoe Area Wilderness	−0.13	0.08	0.51	0.14	−0.02	0.08	−0.02	−47.29	0.00	0.04	0.03	0.01	4.00E−04	↑
Aoraki Mackenzie	−0.06	0.07	0.39	0.08	0.06	0.09	0.05	5.64	0.00	0.05	0.02	0.93	0.00E+00	–
Grand Canyon National Park	−0.06	0.01	0.29	0.06	0.00	0.00	0.00	2.33	0.00	0.01	0.00	0.73	0.00E+00	–
Cévennes National Park Buffer Zone	0.06	0.28	0.71	0.13	0.25	0.21	0.27	−1.90	0.00	0.32	0.03	0	−9.00E−04	↓

The dataset spans inclusively from 2012 to 2022. Statistics are based on monthly radiance values. Min, Max, Ave, σ: Basic statistics of the whole dataset for the given time span; 2012 and 2022: Average of initial and final years of the dataset; APV: Averaged pixel value of the dataset; AAD: Averaged annual development (%); Linear regression parameters (slope "a" and intercept "b") and R^2 values are also provided. The Mann–Kendall (MK) test results and change trend (Q) indicate whether the sky quality is improving (↑), declining (↓) or stable (-). Values less than 0.01 are shown as 0.0

IDS Sanctuary, they are not appropriate for IDS Parks or IDS Reserves. Another key goal of the programme, the promotion of effective lighting technologies, can only be achieved in locations where lighting is actually needed. Although protecting existing dark areas remains important, the IDSP may not be the most suitable approach for such regions. A recent study by Pan et al. (2025) for China provides relevant recommendations for the programme criteria.

4 Conclusion

In this study, the temporal variations of light pollution in IDSP are analysed using different statistical and machine learning methods. The main outputs of our study are listed below:

The global locations of IDSPs appear to be closer to clustered bright areas in North America and European countries. Where ALAN is relatively low (in deserts or mountains), there are no IDSPs due to transportation and human access. According to the linear regression analysis covering the years 2012–2022, 94% of IDSPs did not show any change in ALAN. Only 3% of 216 IDSPs showed a decrease in light pollution. In AAD values, 151 locations out of 216 IDSPs are above 0.5.

According to Mann–Kendall and Sen's slope statistics for this dataset, the ALAN levels of 144 locations showed a significant change over time in 105 locations, 78 show an increasing trend, while 27 show a decreasing trend. A total of 12 different regression models, including machine learning techniques, were applied to the monthly average data. Among these methods, the DTR, RFR and GBR techniques gave better prediction results ($R^2 > 0.6$) than the others. To determine the seasonal effects of ALAN increases, the LS periodogram was used to determine the best frequency values for all sites. Although periodic patterns were detected as a result, these were considered false positives as the values were consistent with the monthly sampling interval.

We highlighted the need to carefully assess the trends in light pollution, particularly in IDSP areas. Although light pollution is increasing globally, our findings indicate that the rate of increase in IDSP areas is slower compared to non-IDSP regions, underscoring the effectiveness of existing conservation strategies. However, the notion that IDSPs are entirely free from light pollution is not always accurate. Our results reveal that some IDSPs still experience significant levels of light pollution, suggesting that current control measures may be insufficient and stronger regional strategies are needed. In conclusion, although light pollution cannot be completely eliminated in IDSPs, their lower pollution rates compared to other areas highlight their importance as benchmarks for dark night sky preservation. Future research should further evaluate the effectiveness of protection policies and focus on expanding successful strategies to broader regions.

4.1 Final note on protecting the darkness

The protection of IDSPs is of critical importance for both environmental sustainability and astronomical observations. To ensure their preservation, it is essential to

Table 3 Statistical models R^2 score comparison

Places	PR	Ridge	Lasso	EN	SVR	DTR	RFR	GBR	ABR	KNR	BR
Greater Big Bend International Dark Sky Reserve	0.43	0.43	0.43	0.43	−0.18	0.88	0.85	0.85	0.66	0.63	0.43
Death Valley National Park	0.01	0.00	0.00	0.00	−0.53	0.77	0.60	0.71	0.28	−0.08	0.00
Oregon Outback (Lake County, Phase One)	0.06	0.06	0.06	0.06	−0.01	−0.11	0.35	0.05	−0.15	0.22	0.06
Kerry	0.03	0.02	0.02	0.02	0.00	0.84	0.75	0.79	0.29	0.10	0.02
Quetico Provincial Park	0.04	0.03	0.03	0.03	0.01	0.53	0.62	0.61	0.22	0.09	0.03
Mont-Mégantic	0.00	0.00	0.00	0.00	−0.10	0.79	0.78	0.77	0.12	0.28	0.00
Boundary Waters Canoe Area Wilderness	0.04	0.03	0.03	0.03	0.04	0.53	0.60	0.59	0.20	0.07	0.03
Aoraki Mackenzie	0.02	0.01	0.01	0.01	−0.04	0.63	0.56	0.64	0.41	0.18	0.01
Grand Canyon National Park	0.01	0.00	0.00	0.00	−0.34	0.87	0.66	0.84	0.32	−0.07	0.00
Cévennes National Park Buffer Zone	0.03	0.01	0.01	0.01	−0.01	0.77	0.75	0.77	0.40	0.16	0.01

11 statistical models were used: PR: polynomial regression, EN: ElasticNet, DTR: decision tree regressor, RFR: random forest regressor, GBR: gradient boosting regressor, ABR: AdaBoost regressor, KNR: K neighbour regressor, BR: Bayesian Ridge. IDSPs are selected according to their light pollution change slope. R^2 values are multiplied by 100 for better readability

Table 4 Period (in months), power and FAP information for 10 IDSPs obtained using the LS periodogram method

Places	Period	Power	FAP
Greater Big Bend International Dark Sky Reserve	0.50	0.00	0.50
Death Valley National Park	0.48	0.00	0.27
Oregon Outback (Lake County, Phase One)	0.48	0.00	0.19
Kerry	0.48	0.00	0.41
Quetico Provincial Park	0.48	0.00	0.42
Mont-Mégantic	0.48	0.00	0.64
Boundary Waters Canoe Area Wilderness	0.48	0.00	0.42
Aoraki Mackenzie	0.46	0.01	0.18
Grand Canyon National Park	0.48	0.00	0.35
Cévennes National Park Buffer Zone	0.48	0.00	0.32

raise public awareness of the responsible use of artificial light in and around these areas. In this regard, the state of Arizona serves as a notable example, implementing effective policies and community initiatives aimed at reducing light pollution (Alva et al. 2025). In addition, public authorities must play an active role in safeguarding these designated regions through legal and administrative measures. For example, despite there being no final verdict on the INNA project ESO (2025), the Chilean government has taken significant steps to protect the site of one of the world's largest observatories located in the Andes Mountains (NOIRLab 2023). Furthermore, for long-term effectiveness, education on artificial light usage and its environmental impacts should be incorporated into school curricula starting from the primary level.

Abbreviations

AAD	Averaged annual development
ABR	AdaBoost regressor
ALAN	Artificial light at night
AVP	Averaged pixel value
BR	Bayesian ridge
DNB	Day–night band
DTR	Decision tree regression
EN	ElasticNet
GBR	Gradient boosting regression
GIS	Geographical information system
IDSPs	International Dark-Sky Places
KNR	K neighbour regressor
LS	Lomb–Scargle
MK	Mann–Kendall
PR	Polynomial regression
Q	Sen's slope coefficient
RFR	Random forest regression
SQM	Sky quality meter
Suomi NPP	Suomi National polar-orbiting partnership
VIIRS	Visible infrared imaging radiometer suite
VNL	VIIRS nighttime lights

Acknowledgements
During the preparation of this work, the author(s) utilised ChatGPT—3.5 to refine the English wording of certain phrases. Following the use of this tool, the author(s) reviewed and edited the content as necessary and took full responsibility for the content of the publication. The views expressed in this article are solely MB own and do not represent the official position of my affiliated institution.

Author contributions
NA and ZK handled data download and organisation. MB and MAE used geographical information systems in the study. SKY contributed to structural editing and evaluation. All authors reviewed and edited the manuscript.

Funding
This research was supported by the Scientific and Technological Research Council of Turkey (TÜBİTAK) through project number 123F244.

Availability of data and materials
The datasets supporting the conclusions of this article are included within the article and its additional files.

Declarations

The views expressed in this article are solely those of Murat Bayazıt and do not represent the official position of his affiliated institution.

Competing interest
The authors declare that they have no Conflict of interest.

Received: 19 February 2025 Accepted: 17 July 2025
Published: 12 January 2026

References

Aksaker N, Yerli SK, Kurt Z, Bayazit M, Aktay A, Erdoğan MA (2020) A case study of light pollution in France. Ap &SS 365(9):153. https://doi.org/10.1007/s10509-020-03869-4. arXiv:2006.04440

Altman N, Krzywinski M (2017) Ensemble methods: bagging and random forests. Nat Methods 14(10):933–935

Alva A, Brown E, Evans A, Morris D, Dunning K (2025) Dark sky parks: public policy that turns off the lights. J Environ Plann Manag 68(4):907–934. https://doi.org/10.1080/09640568.2023.2275535

Amaral S, Monteiro A, Câmara G, Quintanilha JA (2006) DMSP/OLS night-time light imagery for urban population estimates in the Brazilian amazon. Int J Remote Sens 27(5):855–870

Argys LM, Averett SL, Yang M (2021) Light pollution, sleep deprivation, and infant health at birth. South Econ J 87(3):849–888

Baluev RV (2008) Assessing the statistical significance of periodogram peaks. MNRAS 385(3):1279–1285. https://doi.org/10.1111/j.1365-2966.2008.12689.x. arXiv:0711.0330

Barentine J (2016) Going for the gold: quantifying and ranking visual night sky quality in international dark sky places. Int J Sustain Light 18:9–15

Barentine JC, Kundracik F, Kocifaj M, Sanders JC, Esquerdo GA, Dalton AM, Foott B, Grauer A, Tucker S, Kyba C (2020) Recovering the city street lighting fraction from skyglow measurements in a large-scale municipal dimming experiment. J Quant Spec Radiat Transf 253:107120. https://doi.org/10.1016/j.jqsrt.2020.107120. arXiv:2005.12357

Barentine JC, Walczak K, Gyuk G, Tarr C, Longcore T (2021) A case for a new satellite mission for remote sensing of night lights. Remote Sens 13(12):2294. https://doi.org/10.3390/rs13122294

Basak D, Pal S, Patranabis DC et al (2007) Support vector regression. Neural Inf Process Lett Rev 11(10):203–224

Cao C, Bai Y (2014) Quantitative analysis of VIIRS DNB nightlight point source for light power estimation and stability monitoring. Remote Sens 6(12):11915–11935

Cao C, Bai Y (2014) Quantitative analysis of VIIRS DNB nightlight point source for light power estimation and stability monitoring. Remote Sens 6(12):11915–11935. https://doi.org/10.3390/rs61211915

Cao M, Xu T, Yin D (2023) Understanding light pollution: recent advances on its health threats and regulations. J Environ Sci 127:589–602

Cinzano P, Falchi F, Elvidge C, Baugh K (2000) The artificial night sky brightness mapped from DMSP satellite operational linescan system measurements. Mon Not R Astron Soc 318(3):641–657

Coesfeld J, Kuester T, Kuechly HU, Kyba C (2020) Reducing variability and removing natural light from nighttime satellite imagery: a case study using the VIIRS DNB. Sensors 20(11):3287. https://doi.org/10.3390/s20113287

Conover WJ (1999) Practical nonparametric statistics. Wiley Series in Probability and Statistics. Wiley, New York

Elvidge CD, Baugh KE, Zhizhin M, Hsu F-C (2013) Why VIIRS data are superior to DMSP for mapping nighttime lights. Proc Asia-Pac Adv Netw 35:62

Elvidge CD, Hsu F-C, Zhizhin M, Ghosh T, Taneja J, Bazilian M (2020) Indicators of electric power instability from satellite observed nighttime lights. Remote Sens 12(19):3194. https://doi.org/10.3390/rs12193194

Elvidge CD, Zhizhin M, Ghosh T, Hsu F-C, Taneja J (2021) Annual time series of global viirs nighttime lights derived from monthly averages: 2012 to 2019. Remote Sens 13(5):922. https://doi.org/10.3390/rs13050922

Escario-Sierra F, Álvarez-Alonso C, Moseñe-Fierro JA, Sanagustín-Fons V (2022) Sustainable tourism, social and institutional innovation the paradox of dark sky in astrotourism. Sustainability 14(11):6419

E.S.O. (2025) ESO technical analysis confirms planned industrial complex will have extensive impact on paranal observatory. https://www.eso.org/public/news/eso2506/. Accessed on 15 Jul 2025

Falchi F, Cinzano P, Duriscoe D, Kyba CC, Elvidge CD, Baugh K, Portnov BA, Rybnikova NA, Furgoni R (2016) The new world atlas of artificial night sky brightness. Sci Adv 2(6):1600377

Falchi F, Furgoni R, Gallaway TA, Rybnikova NA, Portnov BA, Baugh K, Cinzano P, Elvidge CD (2019) Light pollution in USA and Europe: the good, the bad and the ugly. J Environ Manag 248:109227

Fonken LK, Aubrecht TG, Meléndez-Fernández OH, Weil ZM, Nelson RJ (2013) Dim light at night disrupts molecular circadian rhythms and increases body weight. J Biol Rhythms 28(4):262–271

Gana R (2022) Ridge regression and the lasso: how do they do as finders of significant regressors and their multipliers? Commun Stat Simul Comput 51(10):5738–5772

Gaston KJ, Sánchez de Miguel A (2022) Environmental impacts of artificial light at night. Annu Rev Environ Resour 47(1):373–398

Green RF, Luginbuhl CB, Wainscoat RJ, Duriscoe D (2022) The growing threat of light pollution to ground-based observatories. A &A Rev 30(1):1. https://doi.org/10.1007/s00159-021-00138-3

Grubisic M, van Grunsven RH, Kyba CC, Manfrin A, Hölker F (2018) Insect declines and agroecosystems: does light pollution matter? Ann Appl Biol 173(2):180–189

Grubisic M, Haim A, Bhusal P, Dominoni DM, Gabriel KM, Jechow A, Kupprat F, Lerner A, Marchant P, Riley W et al (2019) Light pollution, circadian photoreception, and melatonin in vertebrates. Sustainability 11(22):6400

Hänel A, Posch T, Ribas SJ, Aubé M, Duriscoe D, Jechow A, Kollath Z, Lolkema DE, Moore C, Schmidt N et al (2018) Measuring night sky brightness: methods and challenges. J Quant Spectrosc Radiat Transfer 205:278–290

He Y, Wang A, Huang H (2013) The trend of natural illuminance levels in 14 Chinese cities in the past 50 years. Energy Sustain Soc 3:1–11

Henderson JV, Storeygard A, Weil DN (2012) Measuring economic growth from outer space. Am Econ Rev 102(2):994–1028

Hillger D, Kopp T, Lee T, Lindsey D, Seaman C, Miller S, Solbrig J, Kidder S, Bachmeier S, Jasmin T et al (2013) First-light imagery from suomi npp viirs. Bull Am Meteor Soc 94(7):1019–1029

Iwanicki G (2022) Astro-tourism in the czech-polish izera dark sky park. Handbook of Niche Tourism. Edward Elgar Publishing, UK, pp 2–13

Kendall MG (1975) Rank correlation methods. In: Rank Correlation Methods. Charles Griffin, London, p 160

Kurt Z, Aksaker N, Yerli SK, Erdoğan MA (2024) Investigating potential Dark sky parks in Balkans. Ap &SS 369(84):83. https://doi.org/10.1007/s10509-024-04324-4

Kyba C, Garz S, Kuechly H, de Miguel AS, Zamorano J, Fischer J, Hölker F (2014) High-resolution imagery of earth at night: new sources. Opportunities Challenges Remote Sens 7(1):1–23. https://doi.org/10.3390/rs70100001

Kyba C, Kuester T, Sánchez de Miguel A, Baugh K, Jechow A, Hölker F, Bennie J, Elvidge CD, Gaston KJ, Guanter L (2017) Artificially lit surface of Earth at night increasing in radiance and extent. Sci Adv 3(11):1701528. https://doi.org/10.1126/sciadv.1701528

Kyba CC, Coesfeld J (2021) Satellite observations show reductions in light emissions at international dark sky places during 2012–2020. Int J Sustain Light 23(2):51–57

Kyba CC, Ruhtz T, Fischer J, Hölker F (2011) Cloud coverage acts as an amplifier for ecological light pollution in urban ecosystems. PLoS ONE 6(3):17307

LaRoe J, Holmes CM, Schad T (2022) Nightlight intensity change surrounding nature reserves: a case study in Orbroicher Bruch nature reserve, Germany. Remote Sensing 14(16):3876

Liao L, Weiss S, Mills S, Hauss B (2013) Suomi npp viirs day-night band on-orbit performance. J Geophys Res Atmosph 118(22):12–705

Lima RC, Pinto da Cunha J, Peixinho N (2016) Light pollution: assessment of sky glow on two dark sky regions of Portugal. J Toxicol Environ Health A 79(7):307–319

Liu M, Li W, Zhang B, Hao Q, Guo X, Liu Y (2020) Research on the influence of weather conditions on urban night light environment. Sustain Cities Soc 54:101980

Lomb NR (1976) Least-squares frequency analysis of unequally spaced data. Astrophys Space Sci 39:447–462. https://doi.org/10.1007/BF00648343

Longcore T, Rich C (2004) Ecological light pollution. Front Ecol Environ 2(4):191–198

Mander S, Alam F, Lovreglio R, Ooi M (2023) How to measure light pollution: a systematic review of methods and applications. Sustain Cities Soc 92(92):10–4465. https://doi.org/10.1016/j.scs.2023.104465

Mann HB (1945) Nonparametric tests against trend. Econometrica 13(3):245–259 (**Accessed 2023-09-05**)

Marr NL (2024) Windows to the universe: mapping the values of the galloway forest dark sky park. PhD thesis, University of Glasgow
Martínez-Ledesma M, Sanhueza P, Corco C, Astudillo H, Angeloni R, Damke G, Falchi F, Blanc G (2019) Spectral and Zonal Restriction Justification-Review Process of DS043/2012 MMA (Ministry of Environment). https://doi.org/10.13140/RG.2.2.11949.31206
Mitchell D, Gallaway T (2019) Dark sky tourism: economic impacts on the colorado plateau economy, USA. Tour Rev 74(4):930–942
Mu H, Li X, Du X, Huang J, Su W, Hu T, Wen Y, Yin P, Han Y, Xue F (2021) Evaluation of light pollution in global protected areas from 1992 to 2018. Remote Sens. https://doi.org/10.3390/rs13091849
Natekin A, Knoll A (2013) Gradient boosting machines, a tutorial. Front Neurorobot 7:21
NOIRLab New Light Pollution Regulation Protects Chile's Dark Skies (2023). https://noirlab.edu/public/announcements/ann23034/. Accessed on 15 Jul 2025
Owens AC, Cochard P, Durrant J, Farnworth B, Perkin EK, Seymoure B (2020) Light pollution is a driver of insect declines. Biol Cons 241:108259
Paksarian D, Rudolph KE, Stapp EK, Dunster GP, He J, Mennitt D, Hattar S, Casey JA, James P, Merikangas KR (2020) Association of outdoor artificial light at night with mental disorders and sleep patterns among us adolescents. JAMA Psychiat 77(12):1266–1275
Pan X, Yang D, Wang L, Zhang W, Liu N, Song X, Gao C (2025) A multi-value based approach to identify potential dark sky places in mainland china. Landsc Urban Plan 253:105207. https://doi.org/10.1016/j.landurbplan.2024.105207
Papalambrou A, Doulos LT (2019) Identifying, examining, and planning areas protected from light pollution. the case study of planning the first national dark sky park in greece. Sustainability 11(21):5963
Phan DH (2023) Lights and gdp relationship: what does the computer tell us? Empir Econ 65(3):1215–1252
Pohlert T (2016) Non-parametric trend tests and change-point detection. CC BY-ND 4:1–18
Poole MA, O'Farrell PN (1971) The assumptions of the linear regression model. Transactions of the Institute of British Geographers, 145–158
Puschnig J, Posch T, Uttenthaler S (2014) Night sky photometry and spectroscopy performed at the vienna university observatory. J Quant Spectrosc Radiat Transfer 139:64–75
Rees D, Rees D (1989) Regression analysis. Essential Statistics, 153–166
Rodrigo-Comino J, Seeling S, Seeger MK, Ries JB (2023) Light pollution: a review of the scientific literature. Anthropocene Rev 10(2):367–392
Sainger A, Yadav R, Tipare P, Waghralkar S, Jethani V, Barve A (2020) Analysis of light pollution prediction using mathematical model and machine learning techniques. In: Advanced computing technologies and applications: proceedings of 2nd international conference on advanced computing technologies and applications-ICACTA 2020, pp 31–43. Springer
Sanchez de Miguel A, Kyba CC, Zamorano J, Gallego J, Gaston KJ (2020) The nature of the diffuse light near cities detected in nighttime satellite imagery. Sci Rep 10(1):7829
Scargle JD (1982) Studies in astronomical time series analysis. ii. statistical aspects of spectral analysis of unevenly spaced data. Astrophys J 263:835–853. https://doi.org/10.1086/160554
Schirmer AE, Gallemore C, Liu T, Magle S, DiNello E, Ahmed H, Gilday T (2019) Mapping behaviorally relevant light pollution levels to improve urban habitat planning. Sci Rep 9(1):11925
Schwarzenberg-Czerny A (1998) The distribution of empirical periodograms: Lomb-scargle and pdm spectra. Mon Not R Astron Soc 301(3):831–840
Sen PK (1968) Estimates of the regression coefficient based on kendall's tau. J Am Stat Assoc 63(324):1379–1389
Singhal RK, Kumar M, Bose B (2019) Eco-physiological responses of artificial night light pollution in plants. Russ J Plant Physiol 66:190–202
Spinner R, Kuechly H, Necsulescu D, Hartley R, Scisco M, Kyba C (2024)Administrative boundaries of selected certified International Dark Sky Places. GFZ DataServices. https://doi.org/10.5880/GFZ.1.4.2024.005
Sun N, Zhu F, Wang X (2024) Research on light pollution evaluation modeling based on comprehensive weights. Highlights Sci Eng Technol 94:611–618
Sysoev O, Burdakov O (2019) A smoothed monotonic regression via l2 regularization. Knowl Inf Syst 59:197–218
Wallner S, Kocifaj M (2023) Aerosol impact on light pollution in cities and their environment. J Environ Manag 335:117534
Wallner S, Puschnig J, Stidl S (2023) The reliability of satellite-based lighttrends for dark sky areas in austria. J Quant Spectrosc Radiat Transfer 311:108774. https://doi.org/10.1016/j.jqsrt.2023.108774
Xiang W, Tan M (2017) Changes in light pollution and the causing factors in China's Protected Areas, 1992–2012. Remote Sensing. https://doi.org/10.3390/rs9101026
Yerli SK, Aksaker N, Bayazit M, Kurt Z, Aktay A, Erdoğan MA (2021) The temporal analysis of light pollution in Turkey using VIIRS data. Ap &SS 366(4):34. https://doi.org/10.1007/s10509-021-03942-6.arXiv:2103.10456
Zamorano J, Tapia C, Pascual S, García C, González R, González E, Corcho O, García L, Gallego J, Sánchez de Miguel A, Solano E, Alacid JM (2019) Night sky brightness monitoring in Spain. In: Montesinos, B, Asensio Ramos, A, Buitrago, F, Schödel, R, Villaver, E, Pérez-Hoyos, S, Ordóñez-Etxeberria, I (eds.) Highlights on Spanish Astrophysics X, pp 599–604
Zhao Z, Li C, He Yu, Li E, Cheng Z (2019) Applications of satellite remote sensing of nighttime light observations: advances, challenges, and perspectives. Remote Sensing 11(17):1971. https://doi.org/10.3390/rs11171971
Zheng S, Chen J, Su Y et al (2023) Research on light pollution based on policy intervention optimization model. Acad J Environ Earth Sci 5(6):59–66
Zou S, Zhang J, Li L (2023) Random forest-topsis based light pollution evaluation system. Highlights Sci Eng Technol 64:74–80
Zubidat AE, Haim A (2017) Artificial light-at-night-a novel lifestyle risk factor for metabolic disorder and cancer morbidity. J Basic Clin Physiol Pharmacol 28(4):295–313

Publisher's Note

Springer Nature remains neutral with regard to jurisdictional claims in published maps and institutional affiliations.